Pithecellobium dulce as efficient and sustainable source for biosynthesis of NiO nanoparticles with promising potential for degradation of Malachite green and antibacterial activity

Ganesh Kumar Pidugu[1,2], Kethavath Bharath Kumar Naik[3], Rama Rao Vangara[1,2], V. Siddaiah[1*]

[1]Dept. of Chemistry, Andhra University, Visakhapatnam-530017, India
[2]Dept. of Chemistry, Maharajah's College (A), Vizianagaram-535002, India
[3]Govt. Degree College, Araku Valley, Alluri Sitaramaraju District, AP-531149, India

Abstract
This study reports the sustainable biosynthesis of nickel oxide nanoparticles (NiO NPs) using *Pithecellobium dulce* leaf extract as a natural reducing and stabilizing agent. Characterization via XRD, SEM, and EDX confirmed the formation of pure, hexagonal-crystalline NiO NPs with an average crystallite size of 12.49 nm and a particle size of 27.56 nm. Optical analysis revealed a direct band gap of 2.8 eV, while TGA demonstrated exceptional thermal stability up to 931°C. The synthesized nanoparticles exhibited potent, concentration-dependent antibacterial activity against both Gram-positive and Gram-negative pathogens. Furthermore, the NiO NPs functioned as an efficient photocatalyst, achieving 100% degradation of Malachite Green dye within 60 minutes under visible light at optimized conditions (pH 9, 60 mg dosage). These results highlight the potential of P. dulce-mediated NiO NPs as high-performance materials for environmental remediation and biomedical applications.

Keyword: NiO NPs, Malachite Green, *Pithecellobium dulce,* Photocatalysis and Antibacterial activity.

1. Introduction

In recent years, rapid population growth and industrial advancements have led to the excessive release of pollutants into the environment, particularly into air and water systems. Among the various sources of water pollution, azo dyes are a major concern. Textile industries and related manufacturing sectors generate large quantities of colored dye effluents that are both toxic and non-biodegradable [1,2]. To address this growing problem, nanotechnology has emerged as a promising tool, offering advanced solutions for water purification. Nanoparticles exhibit distinct biological, mechanical, thermal, electrical, catalytic, and optical properties compared to their bulk counterparts [3,4]. In particular, metal oxide nanoparticles have gained significant attention for their potential in bioremediation and the treatment of wastewater contaminated with organic and inorganic pollutants [5,6]. Dye degradation using metal oxide nanoparticles such as ZnO, CuO, TiO_2, CdO, and NiO has been recognized as an economical and effective approach for removing organic contaminants from industrial effluents [7,8]. Among these materials, nickel oxide (NiO) is a p-type semiconductor with a wide band gap of 3.6-4.0 eV, stands out due to its high chemical and thermal stability, excellent electrochemical performance, and versatile applications in sensors, catalysis, photocatalysis, and biomedical systems [9]. The large surface area-to-volume ratio and strong redox properties of NiO NPs enhance electron transfer reactions, making them highly efficient for environmental remediation and antimicrobial applications.

Conventionally, NiO NPs have been synthesized through chemical and physical routes such as sol-gel, hydrothermal, co-precipitation, solvothermal, and microwave-assisted methods [10,11]. Although these techniques can yield high-quality nanoparticles, they often require toxic precursors, high energy input, and elevated temperatures, leading to potential environmental and biological hazards. Consequently, researchers have turned toward green synthesis is an eco-friendly, cost-effective, and sustainable alternative that utilizes biological reducing agents derived from plants, bacteria, fungi, and algae [12]. Among these, plant-mediated synthesis offers distinct advantages, including biocompatibility, non-toxicity, and the ability of phytochemicals such as flavonoids, terpenoids, polyphenols, and alkaloids to function simultaneously as reducing, capping, and stabilizing agents [3]. Several studies have reported the successful synthesis of NiO NPs using various plant extracts. For example, *Aegle marmelos* leaf extract-mediated NiO NPs demonstrated strong antioxidant and antibacterial activities, attributed to phytoconstituents that facilitated nickel ion reduction and enhanced biological performance [3]. Similarly, *Clitoria ternatea* flower extract, rich in anthocyanins and phenolic compounds, has been shown to act as a powerful reducing and stabilizing agent, producing hexagonal NiO NPs (10-13 nm) with excellent solar-assisted photocatalytic degradation of textile dyes (Fast Green and Rose Bengal) and broad-spectrum antibacterial effects [13]. Moreover, *Senna auriculata* flower extract-based NiO NPs synthesized via a simple aqueous method achieved 97% degradation efficiency of methylene blue under visible light and exhibited strong antibacterial activity against both *Escherichia coli* (Gram-negative) and *Staphylococcus aureus* (Gram-positive), underscoring the role of plant metabolites like phenols, flavonoids, and proteins in nanoparticle formation and stabilization [14]. *Pithecellobium dulce*(commonly known as Manila tamarind), a leguminous plant of the Fabaceae family, is widely distributed across tropical and subtropical regions, including India, Mexico, and the Philippines. Its leaves are abundant in bioactive phytochemicals such as flavonoids, phenolic acids, tannins, alkaloids, saponins, terpenoids,

and glycosides, which contribute to its diverse pharmacological properties. Previous studies have highlighted the strong antioxidant, antimicrobial, anti-inflammatory, and antidiabetic activities of P. dulce, largely attributed to its high polyphenolic and flavonoid content that effectively scavenges free radicals and prevents lipid peroxidation [15,16].

Recently, *Pithecellobium dulce*leaf extract has been extensively used for the green synthesis of various metal oxide nanoparticles, benefiting from its rich reservoir of biomolecules that serve as natural reducing and stabilizing agents. For example, *Pithecellobium dulce*leaf extract has been successfully employed in the biosynthesis of silver (Ag), gold oxide (AuO), and copper oxide (CuO) nanoparticles. The hydroxyl and carbonyl groups present in its phenolic and flavonoid constituents play a crucial role in reducing metal ions and stabilizing the resulting nanoparticles [17–19]. These biogenic nanoparticles have exhibited impressive photocatalytic activity toward organic dye degradation and strong antibacterial properties, highlighting the potential of *Pithecellobium dulce* derived nanomaterials in wastewater treatment and biomedical applications. Furthermore, phytochemicals such as afzelin and kaempferol derivatives present in P. dulce enhance its reducing ability and contribute to the stability and reactivity of the synthesized nanoparticles [20]. Therefore, *Pithecellobium dulce* represents an eco-friendly, renewable, and efficient biological source for the green synthesis of metal oxide nanoparticles with excellent catalytic and antimicrobial potential.In this context, the present study focuses on the green synthesis of nickel oxide nanoparticles using *Pithecellobium dulce*plant leaf extracts as reducing and stabilizing agents, and on exploring their photocatalytic degradation of organic dyes and antibacterial efficacy against pathogenic bacteria. The degradation of the textile dye MG has been chosen to demonstrate the catalytic potential of the green synthesized NiO NPs under visible Additionally, we evaluated the antibacterial activity of NiO NPs against gram- negative bacteria such as *E. coli* and gram-positive bacteria such as *Bacillus subtilis*. There is no research report of *Pithecellobium dulce* leaf extract mediated green synthesis of NiO NPs and application in antibacterial and photocatalytic activity to date.

2. Experimental Section

2.1. Chemicals and Reagents

All chemicals used in this study were of analytical grade and procured from Bio Chem Suppliers, Visakhapatnam. Double-distilled water was utilized for all experimental procedures. The primary reagents included nickel (II) sulfate ($NiSO_4$) and fresh leaves of Pithecellobium dulce, which served as the natural reducing agent for the green synthesis of NiO nanoparticles.

2.2. Sample Collection and Cleaning

Fresh leaves of Pithecellobium dulce were collected from the vicinity of Andhra University, Visakhapatnam (Coordinates: 17.7230928, 83.3246684) and authenticated by a local taxonomist. The collected leaves were thoroughly washed with distilled water three times, disinfected using a dilute $HgCl_2$ solution, and rinsed again to remove any residual contaminants. The leaves were then shade-dried at room temperature for seven days to preserve their phytochemical constituents.

2.3. Preparation of Leaf Extract

The air-dried leaves were finely powdered using a domestic grinder. Approximately 2 g of the powdered material was transferred into a 250 mL beaker containing 100 mL of distilled water and heated at 70°C for 1 hour to extract the bioactive compounds. The resulting mixture was cooled to room temperature and filtered through Whatman No. 1 filter paper. The filtrate was collected in a volumetric flask, wrapped in aluminum foil to prevent light exposure, and stored at 4°C for subsequent nanoparticle synthesis.

2.4. Green Synthesis of Nickel Oxide Nanoparticles (NiO NPs)

NiO nanoparticles were synthesized using a green co-precipitation method. An aqueous solution of 0.25 M nickel sulfate ($NiSO_4$) was mixed with the prepared Pithecellobium dulce leaf extract in a volumetric ratio of 1:0.75. The solution was stirred magnetically for 10 minutes to promote uniform interaction between metal ions and phytochemicals. To initiate nanoparticle formation, 0.1 M sodium hydroxide solution was added dropwise until the desired pH was achieved. The mixture was then maintained at 80°C under continuous stirring for 90 minutes, leading to the appearance of a dark brown precipitate, confirming the formation of NiO nanoparticles. The precipitate was separated by centrifugation at 4000 rpm for 15 minutes, washed three times with double-distilled water to remove impurities, and dried overnight in a hot air oven at 60°C. The dried product was stored in an airtight container for further characterization and applications.

2.5. Characterization Techniques

The synthesized NiO nanoparticles were characterized using multiple analytical techniques to determine their structural, morphological, elemental, and optical properties. X-ray diffraction (XRD) analysis was performed using a Bruker DX8 diffractometer with a scan rate of 0.02°/s over a 2θ range of 10°–90°. Fourier-transform infrared (FTIR) spectroscopy was carried out on a Shimadzu IR Prestige-21 spectrometer in the range of 500–4000 cm^{-1} to identify functional groups. The morphology and elemental composition were analyzed using a JEOL JSM-6390LA scanning electron microscope (SEM) equipped with an energy-dispersive X-ray (EDX) detector. X-ray photoelectron spectroscopy (XPS) measurements were conducted using an Axis Ultra spectrometer with a

monochromatic Al Kα radiation source. Thermal stability was assessed through thermogravimetric analysis (TGA) using a PerkinElmer STA8000 instrument over a temperature range of 15°C–1000°C.

2.6. Photocatalytic Degradation Experiment

The photocatalytic activity of the green-synthesized NiO nanoparticles was evaluated by examining their ability to degrade malachite green (MG) dye under visible light illumination. In a typical experiment, 50 mL of 10 ppm MG solution was mixed with 50 mg of NiO NPs and stirred in the dark for 30 minutes to achieve adsorption–desorption equilibrium between dye molecules and the catalyst surface. The mixture was then exposed to a 400 W metal halide lamp, simulating visible light at room temperature. At predetermined time intervals, samples were collected and centrifuged at 3000 rpm to separate the catalyst. The absorbance of the clear supernatant was measured at 616 nm using a UV–Vis spectrophotometer to determine the remaining dye concentration. The effects of various parameters, including pH (5-9), irradiation time (0-120 min), catalyst dosage (30-60 mg), and dye concentration (5–20 mg/L), were systematically studied. The degradation efficiency (DE%) was calculated using the standard formula (Equation 1).

$$\boldsymbol{DE\% = \frac{A_o - A_t}{A_t}\, x\, 100} \qquad \boldsymbol{Eq.(1)}$$

Where 'A0' is the initial absorbance of the dye solution and 'At' is the absorbance at a given time 't'.

2.7. Evaluation of Antimicrobial Activity

The antimicrobial activity of the synthesized NiO nanoparticles was evaluated using the agar well diffusion method. Nutrient agar medium was prepared by dissolving 0.8 g of nutrient agar powder in 20 mL of distilled water and sterilized in an autoclave at 121 °C for 20 minutes. For bacterial inoculation, 100 µL each of Escherichia coli and Bacillus subtilis cultures were diluted with 1 mL of sterile distilled water to obtain uniform bacterial suspensions. The sterilized agar medium was poured into sterile Petri dishes and allowed to solidify. Once solidified, the prepared bacterial suspensions were evenly spread over the agar surface to ensure uniform microbial growth. Four wells were then aseptically bored into each plate using a sterile cork borer. One of the wells served as a positive control and was filled with an amoxicillin solution, while the remaining three wells were loaded with NiO nanoparticle suspensions at concentrations of 10 µg/mL, 50 µg/mL, and 100 µg/mL, respectively. The inoculated plates were incubated at 37°C for 48 hours. After incubation, the antimicrobial efficacy of the NiO NPs was determined by measuring the diameter of the inhibition zones around each well, indicating the extent of bacterial growth suppression.

3. Results and discussion

3.1. UV-Visible spectral analysis

The synthesized NiO NPs were analyzed using UV-Visible spectroscopy (Figure 1). The transformation of nickel nitrate solution into NiO NPs was confirmed through spectral analysis in the wavelength range of 200-800 nm. A distinct absorption peak was observed at 252 nm in the UV region, indicating the successful formation of NiO nanoparticles. Similar absorption behaviour has been reported by other researchers [21]. The broad absorption tail extending up to 700–800 nm may be attributed to sub-bandgap transitions and the presence of defect states or surface plasmon resonance effects, which are characteristic features of nanoscale NiO resulting from quantum confinement [22,23].

The energy band-gap of these nanoparticles is assessed utilizing the Tauc-equation [24]. In Tauc-equation $(\alpha h\upsilon)^2$ where α is absorption coefficient, hυ is the photon energy, Eg is the bandgap n = 2 for the indirect transitions. A plot of $(\alpha h\upsilon)^2$ versus hυ is shown in the inset of Figure 4 and the linear portion of the curve is extrapolated to the hυ axis to determine the band-gap. The band gap energy of the synthesized NiO nanoparticles was determined to be 2.8 eV, which is consistent with previously reported values [25,26]. This value is lower than that of bulk NiO (3.6-4.0 eV), primarily due to the quantum confinement effect observed at the nanoscale [27]. The obtained band gap confirms the semiconducting nature of the NiO NPs and falls within the range typical of highly efficient photovoltaic materials. Hence, the observed band gap value indicates that the synthesized NiO nanoparticles are promising candidates for use in optoelectronic devices, photocatalytic processes, and energy storage applications.

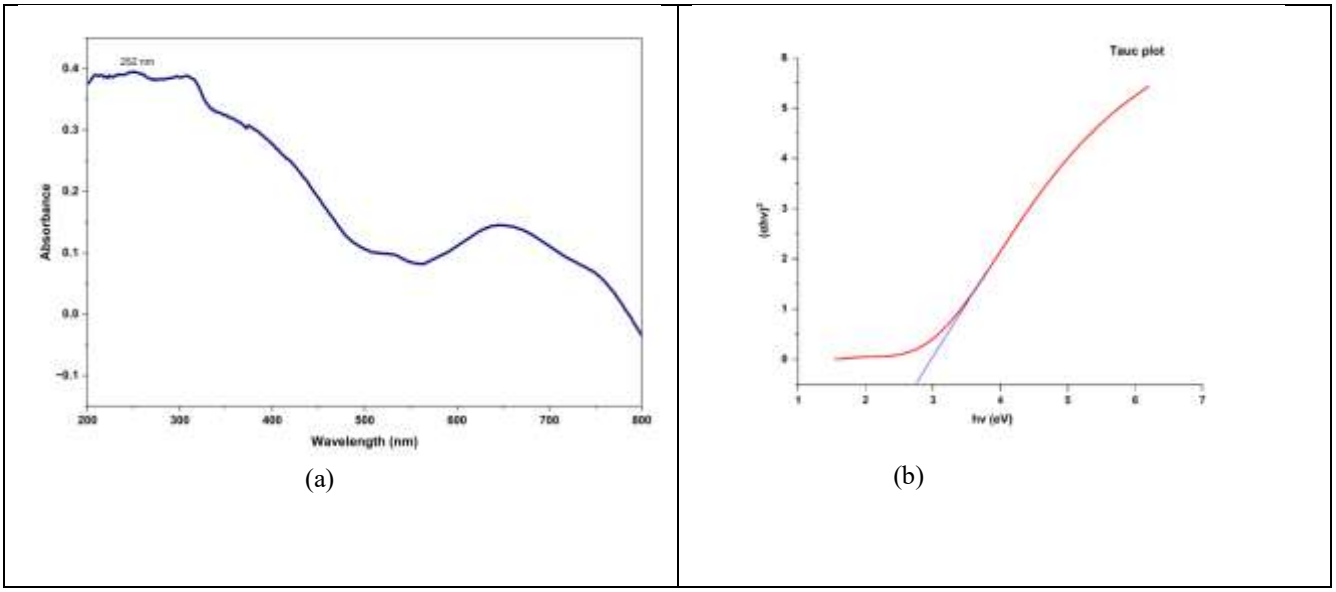

(a) (b)

Fig.1: (a) UV–visible, and (b) optical bandgap energy spectra of biosynthesized NiO NPs

3.2. FTIR analysis

Figure 1a presents the FT-IR spectrum of the synthesized NiO nanoparticles, displaying several prominent absorption peaks at 3379, 3118, 2360, 1720, 1525, 1400, 1174, and 599 cm^{-1}. The broad peaks at 3379 cm^{-1} and 3118 cm^{-1} correspond to O-H stretching vibrations of hydroxyl groups and adsorbed water molecules on the nanoparticle surface, which are characteristic of metal oxide nanostructures due to their high surface area and hydrophilic nature. These bands may also be associated with the O-H stretching of hydrogen-bonded carboxylic acids or the presence of aldehyde or carboxylic functional groups, indicating residual organic components from the plant extract used during synthesis. The absorption band at 2596 cm^{-1} corresponds to C-H stretching, while the peak observed at 2360 cm^{-1} arises from asymmetric stretching of CO_2 molecules. A sharp band at 1720 cm^{-1} is attributed to the C=O stretching vibrations of carbonyl groups. The peaks at 1525 cm^{-1} and 1400 cm^{-1} represent C=C stretching and O-H bending vibrations of aromatic or phenolic compounds, respectively. The absorption at 1174 cm^{-1} corresponds to C–O stretching, confirming the presence of alcohols and carboxylic acid groups that play a role in the reduction and stabilization of NiO nanoparticles [28]. The bands appearing at 742 cm^{-1} and 599 cm^{-1} are assigned to Ni-O bond vibrations, confirming the successful formation of nickel oxide. The presence of these organic functional groups across the spectrum indicates the partial retention of biomolecules from the *Pithecellobium dulce* extract, which enhances the stability and surface functionality of the synthesized nanoparticles [13].

3.3. XRD analysis

Figure 1b displays the X-ray diffraction (XRD) pattern of the synthesized NiO NPs, showing intense and sharp peaks that confirm their high crystallinity and phase purity. The diffraction peaks observed at 2θ values of 19.25°, 31.75°, 33.3°, 38.55°, 45.5°, and 59.3° correspond to the (101), (100), (110), (111), (200), and (220) crystal planes, respectively, which are in good agreement with the standard cubic NiO phase (JCPDS No. 47-1049) [30]. The average crystallite size of the NiO nanoparticles was estimated using the Debye-Scherrer equation, confirming the nanoscale dimensions of the synthesized material.

$$\boldsymbol{d = 0.9\lambda / \beta\cos\theta} \qquad \textbf{Eq.2}$$

Here, λ represents the X-ray wavelength (1.54 Å), β denotes the full width at half maximum (FWHM) of the diffraction peaks, and θ is the Bragg diffraction angle [30]. The average crystallite size of the NiO nanoparticles was determined to be approximately 12.49 nm. The high crystallinity, along with the reduced particle size and large surface area of the synthesized NiO NPs, is expected to enhance their antibacterial and catalytic performance.

3.4. SEM analysis

The surface morphology of the synthesized NiO NPs was analysed using scanning electron microscopy (SEM). The SEM micrographs presented in Figure 2(a-c) demonstrate a dense aggregation of highly crystalline NiO NPs, confirming their successful formation. The presence of a few larger particles is attributed to the inherent agglomeration behaviour of NiO NPs, which occurs due to their high surface energy and the strong surface tension characteristic of ultrafine nanoparticles. The nanoscale particle size provides a large specific surface area, thereby enhancing the catalytic performance of the NiO NPs. From the SEM analysis, the average cluster diameter of the synthesized NiO nanoparticles was estimated to be approximately 27.56 nm (Figure 2c).

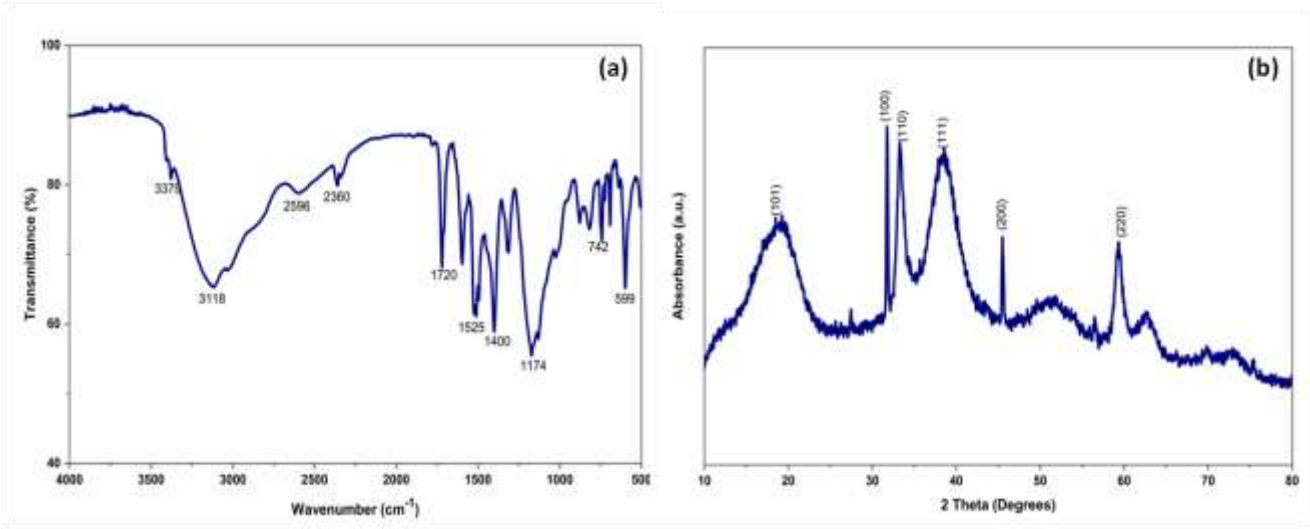

Fig.1: (a) FTIR spectrum, (b) XRD pattern of biosynthesized NiO NPs using *P.dulce* leaf extract

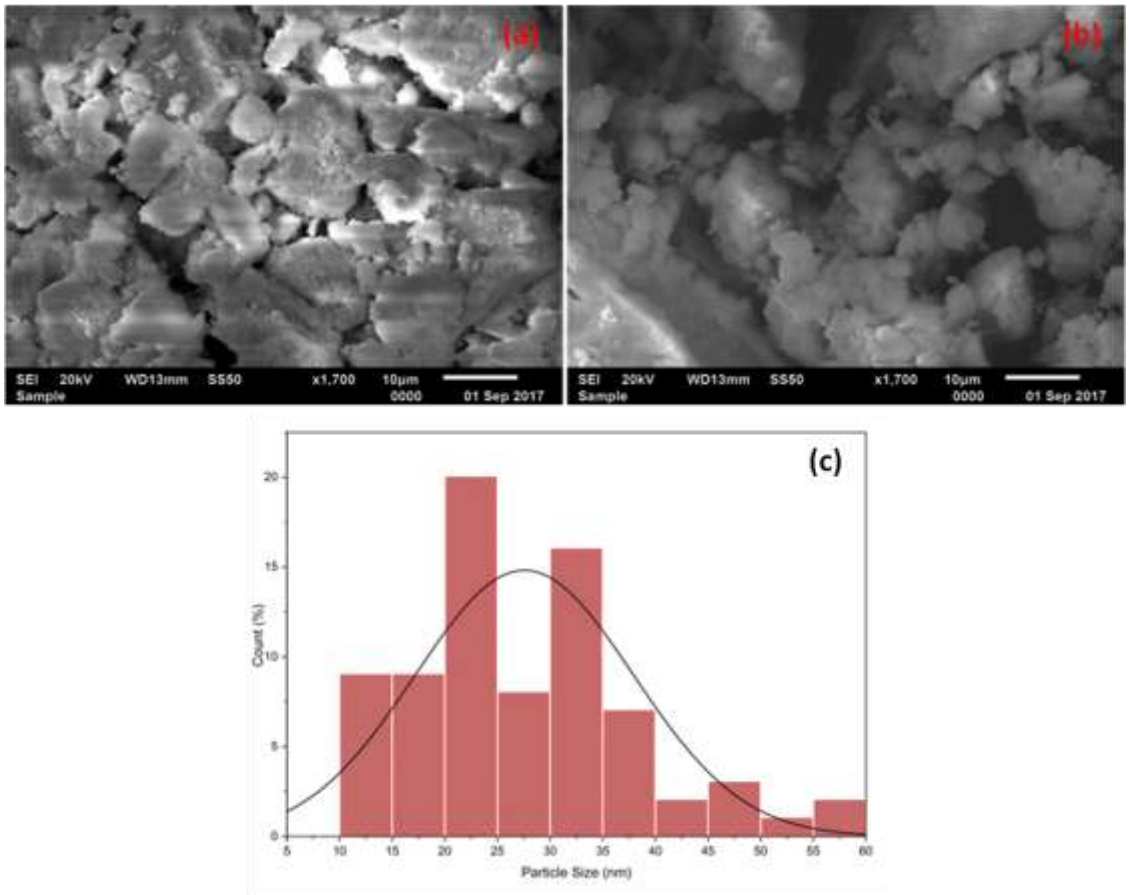

Fig.2: (a-b) SEM image, and (c) particles size of biosynthesized NiO NPs

3.5. XPS analysis

The XPS survey spectrum (Figure 3) exhibits characteristic binding energy peaks corresponding to Ni and O elements present in the synthesized nanoparticles. The Ni 2p spectrum reveals two main peaks associated with Ni $2p_{3/2}$ and Ni $2p_{1/2}$ orbitals. As shown in Figure 3, the characteristic peaks of Ni^{2+} $2p_{3/2}$ and its satellite appear at 854.8 and 860.5 eV, respectively, while the Ni^{2+} $2p_{1/2}$ and its corresponding satellite are observed at 872.6 and 879.5 eV, confirming the formation of NiO structures [33]. The deconvoluted O 1s spectrum displays a dominant peak at 528.8 eV, which corresponds to lattice oxygen in NiO [31], and an additional peak at 531.2 eV attributed to hydroxyl or adsorbed oxygen species on the surface. These XPS results clearly indicate the successful synthesis of NiO NPs with Ni^{2+} as the predominant oxidation state and a surface enriched with hydroxyl and oxygen defect species, which are known to play a crucial role in enhancing their catalytic and adsorption performance [32].

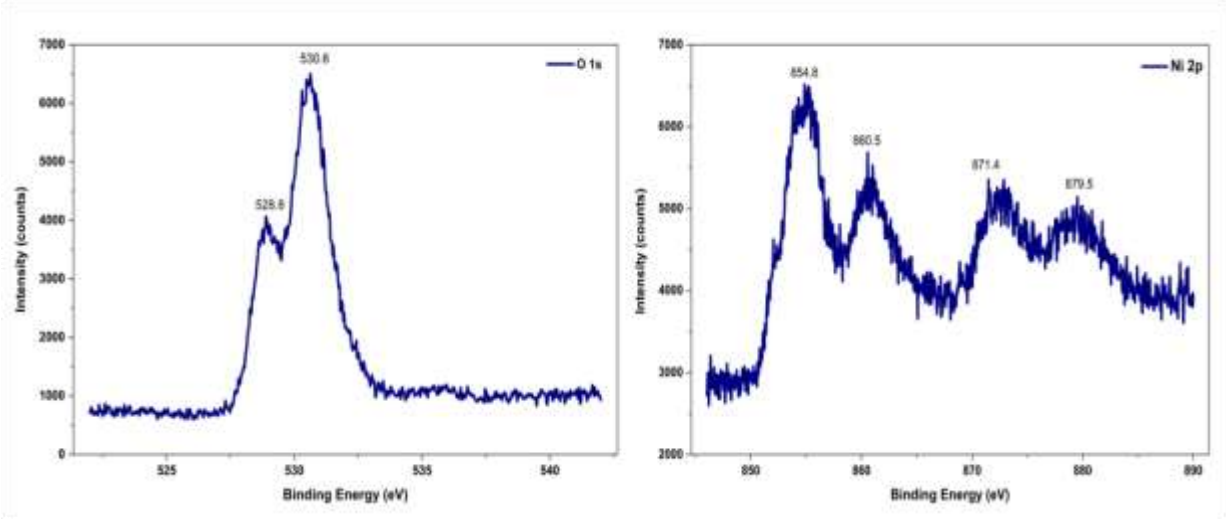

Fig.3: XPS data (a) O1s (b) Ni 2p of biosynthesized NiO NPs

3.6. TGA analysis

To examine the thermal behaviour of the synthesized NiO nanoparticles (NPs) during heat treatment, thermogravimetric analysis (TGA) was carried out in an atmospheric environment over a temperature range of 29–1000°C (Figure 4). The TGA curve reveals three distinct stages of weight loss. The first stage, showing a 16.1 wt% reduction between 29°C and 128°C, is attributed to the evaporation of physically adsorbed and crystallization water molecules. The second significant weight loss of approximately 31.8% observed between 128°C and 303°C corresponds to the decomposition of organic residues and hydroxide precursors such as nickel hydroxide ($Ni(OH)_2$), as well as the removal of other volatile ligands remaining from the biosynthesis process. Beyond 303 ^oC, the curve becomes relatively stable, indicating the elimination of most volatile and organic components and suggesting the onset of NiO crystallization. A gradual weight reduction continues up to around 931^oC, possibly due to the release of tightly bound lattice oxygen or continued densification and phase stabilization of NiO. The overall weight loss of about 42.61% results from the removal and breakdown of organic functional groups present in the biosynthesized sample [33].

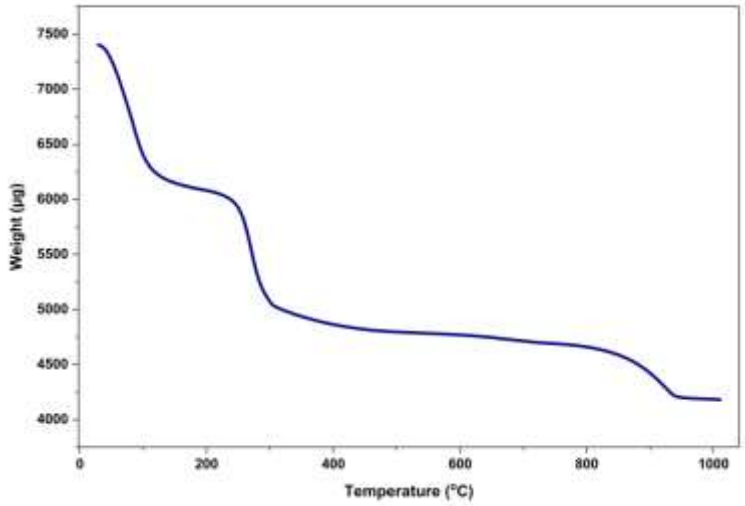

Fig.4: TGA analysis of biosynthesized NiO NPs using

3.7. Photocatalyst activity

Malachite Green (MG) Dye degradation

The photocatalytic efficiency of the synthesized NiO nanoparticles (NPs) was evaluated through the degradation of malachite green (MG) dye under visible light irradiation. Solar light, having a broad continuous spectrum, is not ideal for photocatalysis because only a portion of its spectrum contributes to photoelectron–hole generation. In contrast, visible light provides higher input energy, which is sufficient to excite electrons across the band gap of the photocatalyst [7]. The surface composition of NiO plays a crucial role in dye adsorption, which in turn enhances its photocatalytic performance [24]. Moreover, the physicochemical properties of NiO significantly influence both dye adsorption and subsequent degradation reactions.

The optical absorption spectra of MG dye degradation using NiO NPs are illustrated in Figure 5a. The pristine MG solution exhibits a strong absorption peak at 616 nm, corresponding to the chromophore group of the dye. Upon increasing the visible light irradiation time, the intensity of this peak progressively decreases, indicating the breakdown of chromophoric structures during photocatalytic oxidation.

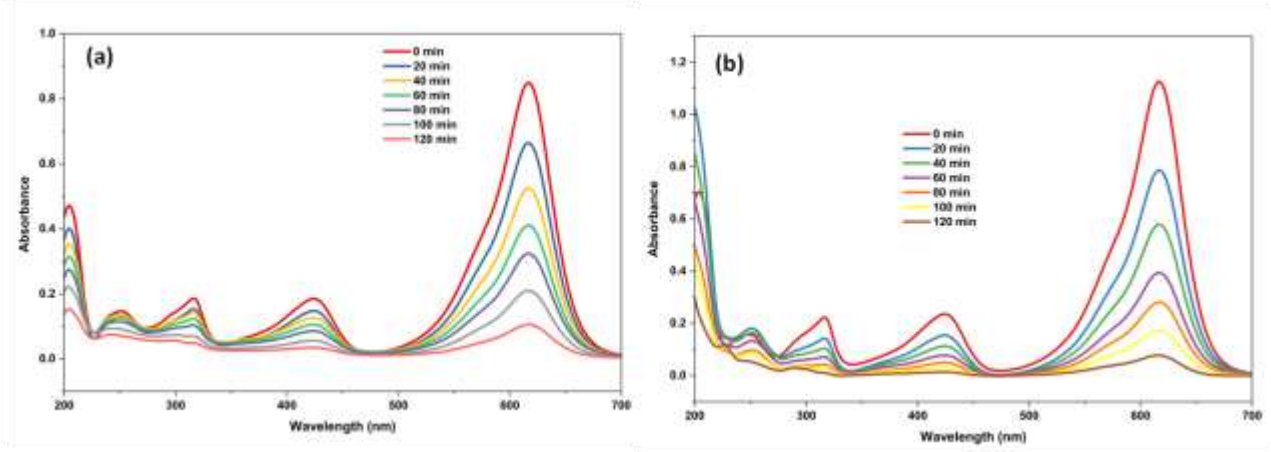

Fig.5: Photocatalytic degradation of MG dye at pH- 7 (a), and pH-9 (b)

It was observed that NiO nanoparticles effectively degraded malachite green (MG) dye under visible light irradiation. At neutral pH (pH 7), NiO nanoparticles achieved an 87.5% degradation of MG dye within 120 minutes (Figure 5a). When the pH was increased to 9, the degradation efficiency further improved to 93.07% within the same duration (Figure 5b). This enhanced photocatalytic performance at alkaline pH can be attributed to the increased formation of hydroxyl radicals (·OH), which serve as the main reactive species responsible for dye oxidation. Under basic conditions, the elevated concentration of hydroxide ions (OH^-) on the NiO surface interacts with photogenerated holes to produce a greater number of ·OH radicals, thereby accelerating the degradation process. Moreover, at pH 9, the negatively charged NiO surface enhances electrostatic attraction toward the cationic MG dye molecules, facilitating improved dye adsorption onto the catalyst surface and promoting faster photodegradation. Thus, the synergistic effects of enhanced adsorption and increased ·OH radical generation result in superior photocatalytic activity of NiO nanoparticles under alkaline conditions.

a) Effect of Catalyst Loading

Further optimization was performed by varying the catalyst dosage from 30 mg to 60 mg while maintaining a constant MG dye concentration of 10 ppm and pH 9. The corresponding results are presented in Figure 6a. As the catalyst loading increased, a gradual enhancement in degradation efficiency was observed, reaching a maximum at approximately 60 mg of NiO nanoparticles. This improvement can be attributed to the higher availability of active sites and increased photon absorption on the catalyst surface, which collectively enhance the photocatalytic degradation process. Additionally, greater light penetration into the suspension and prolonged reaction time further contributed to the enhanced degradation efficiency. Similar trends have been reported by Salarian et al. [34].

b) Dye initial concentration

The photocatalytic degradation of malachite green (MG) dye is a complex process influenced by several parameters, including the solution pH, catalyst dosage, and initial dye concentration. One of the key factors affecting degradation efficiency is the blanket effect, which occurs when dye molecules become so concentrated that they cover the active sites on the surface of the nanoparticles, thereby hindering photocatalytic activity.

In the present study, the optimum initial MG dye concentration for effective degradation was found to be 10 mg/L, where the influence of the blanket effect remained minimal, and the degradation rate was relatively high. As illustrated in Figure 6b, the degradation efficiency decreases progressively with an increase in the initial dye concentration. At a low concentration of 5 mg/L, nearly 100% degradation of MG dye was achieved, demonstrating the strong photocatalytic performance of NiO under these conditions. However, as the dye concentration increased to 10 mg/L and 15 mg/L, the degradation efficiency declined slightly to 94.5% and 91.2%, respectively. A more significant drop was observed at 20 mg/L, with only about 78.3% degradation efficiency.

This reduction in degradation efficiency at higher dye concentrations can be attributed to the saturation of active sites on the NiO surface and the limited availability of reactive species. At lower concentrations, the catalyst surface provides ample active sites and effective light penetration, ensuring efficient generation of reactive radicals for dye degradation. In contrast, higher concentrations lead to competition among dye molecules for active sites and cause excessive light absorption by the dye itself, thereby reducing photon availability for photocatalysis. Consequently, both surface site saturation and restricted light penetration contribute to the observed decrease in degradation efficiency at elevated dye concentrations.

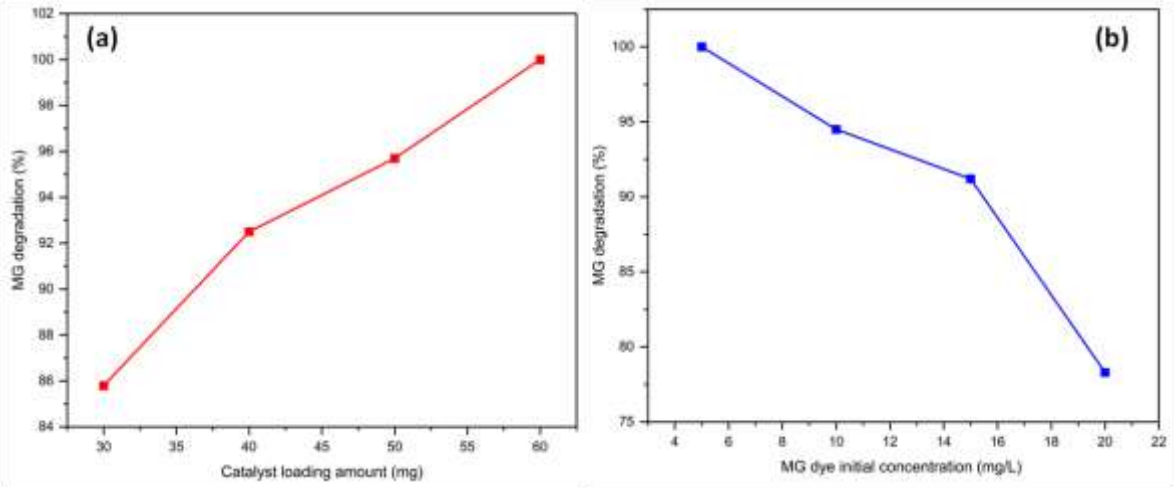

Fig.6: Effect of dosage of catalyst (a), and MG dye initial concentration (b) on the photocatalytic degradation efficiency of biosynthesized NiO NPs

3.8. Antibacterial activity

The antibacterial potential of green-synthesized NiO NPs was assessed against both Gram-positive (*Bacillus subtilis*, MTCC-441) and Gram-negative (*Escherichia coli*, MTCC-589) bacterial strains using the agar well diffusion method. As illustrated in Figure 7, NiO NPs exhibited a distinct inhibitory effect against both bacterial species, with the zone of inhibition increasing proportionally with nanoparticle concentration. The corresponding data are summarized in Table 1. For *B. subtilis*, the mean inhibition zones were recorded as 9 mm, 10 mm, and 12 mm at concentrations of 10 µg/mL, 50 µg/mL, and 100 µg/mL, respectively, while the control exhibited a zone of 17 mm. Similarly, *E. coli* showed inhibition zones of 10 mm, 10 mm, and 12 mm at the same respective concentrations, compared with 16 mm for the control. These results confirm that the green-synthesized NiO NPs possess broad-spectrum antibacterial activity effective against both Gram-positive and Gram-negative bacteria, and that the antibacterial efficacy increases with nanoparticle concentration.

The observed antibacterial activity of green-synthesized NiO NPs can be attributed to multiple mechanisms. Phytochemicals present in the plant extracts used during synthesis serve as natural capping and reducing agents, improving nanoparticle stability and enhancing biological compatibility [35]. The nanoscale size and high surface area of the NiO NPs promote strong interaction with bacterial cell membranes, resulting in structural disruption, membrane damage, and leakage of intracellular contents. Furthermore, NiO NPs are known to generate reactive oxygen species (ROS), such as hydroxyl radicals (•OH) and superoxide anions (O_2•$^-$), which cause oxidative stress, leading to damage of essential biomolecules including proteins and DNA, ultimately resulting in bacterial cell death [3].

Several previous studies have reported similar antibacterial efficacy of green-synthesized NiO nanoparticles. For example, Sathishkumar et al. (2019) demonstrated that NiO NPs synthesized using *Azadirachta indica* (neem) leaf extract exhibited strong antibacterial activity *against E. coli* and *Staphylococcus aureus*, surpassing that of chemically synthesized NiO NPs [36]. Likewise, Sukumaran et al. (2025) reported that NiO NPs synthesized from *Aegle marmelos* extract displayed enhanced antibacterial performance due to increased ROS generation and nickel ion release [3]. The present findings are consistent with earlier reports, confirming that green-synthesized NiO nanoparticles possess potent antibacterial activity and can serve as effective antimicrobial agents. The utilization of plant extracts not only provides an eco-friendly and cost-effective synthesis route but also enhances biological efficacy through synergistic interactions between phytochemicals and NiO. Hence, green-synthesized NiO NPs hold significant promise for diverse applications, including biomedical coatings, wound healing materials, water purification, and environmental disinfection.

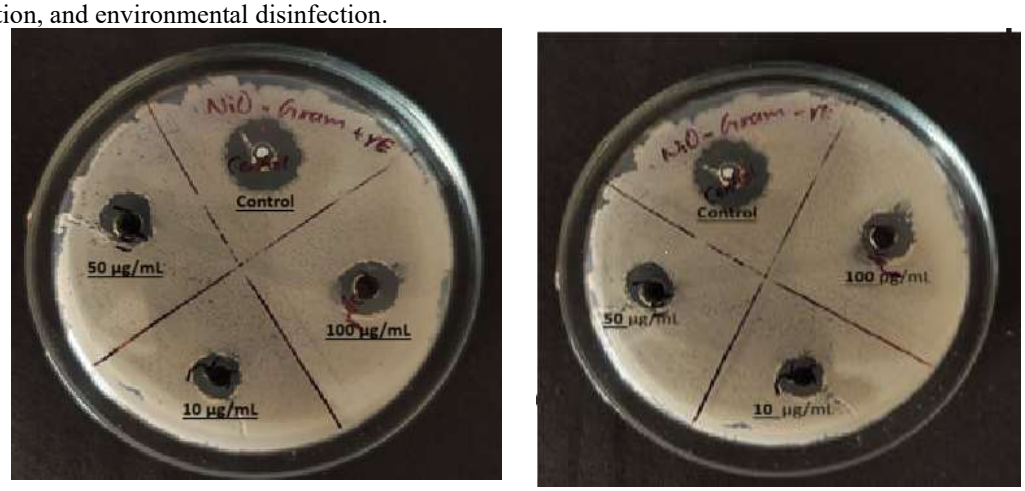

Fig. 7: Antibacterial activity of nickel oxide nanoparticles against bacteria (a) *B.subtilis*, (b) *E.coli*

Table 1: The zone of inhibition of NiO NPs suing *P.dulce* leaf extract

Microorganism	Average zone of inhibition in nm			
	10µg/mL	50µg/mL	100µg/mL	Control
B.subtilis	9mm	10mm	12mm	17mm
E.coli	10mm	10mm	12mm	16mm

Conclusion

In this study, NiO NPs were successfully synthesized using *Pithecellobium dulce* extract for the first time. The synthesized NiO NPs exhibited an optical band gap of 2.8 eV, confirming their p-type semiconducting nature, which makes them suitable candidates for photocatalytic and antibacterial applications. FTIR analysis confirmed the effective role of the plant extract as a natural stabilizing and capping agent during nanoparticle formation. SEM micrographs revealed uniformly agglomerated NiO NPs with an average size of approximately 27.6 nm. The antibacterial assays demonstrated that the NiO NPs possess strong inhibitory activity against both *Bacillus subtilis* and *Escherichia coli*. Furthermore, the NiO NPs exhibited excellent photocatalytic performance in the degradation of malachite green (MG) dye under visible light irradiation without the need for any external energy source. Based on these findings, the green-synthesized NiO NPs show great potential for use in cost-effective industrial wastewater treatment and various antibacterial or biomedical applications.

References

1. Z. Monsef Khoshhesab, K. Gonbadi, G. Rezaei Behbehani, Removal of reactive black 8 dyefrom aqueous solutions using zinc oxide nanoparticles: investigation of adsorption param eters. Desalin Water Treat 56(6), 1558–1565 (2015) 17.
2. G. Mezohegyi et al., Advanced bioreduction of commercially important azo dyes: modeling and correlation with electrochemical characteristics. Ind. Eng. Chem. Res. 48(15), 7054–7059 (2009)
3. Jawahar Sukumaran, Manogar Priya, Raja Venkatesan, Seong-Cheol Kim, Kiruthika Sathiasivan, Mohammad Rashid Khan. Green Synthesis of Nickel Oxide Nanoparticles Using Leaf Extract of *Aegle marmelos* and Their Antibacterial, Anti- Oxidant, and In Vitro Cytotoxicity Activity. Microscopy Research and Technique, 2025; 88:2830–2842
4. D Tejeswara Rao and P Seetharam. "Synthesis of Quinoline Derivatives Using Double Perovskite Bi1. 97Eu0. 03MoO6 Heterogeneous Nanocatalyst", Russian Journal of Organic Chemistry (Springer)., 2022, 58, 1042-1047.
5. J. Vijayaraghavan, S.S. Basha, J. Jegan, A review on efficacious methods to decolorize reactive azo dye. J. Urban Environ. Eng. 7(1), 30–47 (2013)
6. D.Suresh, G. Vijay Swaroop Singh, T. Appa Rao, M. Rajeswara Rao, B. Dharma Rao, P. Seetharam. "Elimination of Cd (II) from Wastewater using Nickel (II) Tungstate Nanoparticles as Adsorbents: Adsorption Isotherm Study", Journal of chemical health risks, 2023, 13(6), 1944 1953.
7. Sathish Mohan Botsa, P Seetharam, I Manga Raju, P Suresh, G Satyanarayana, Sangaraju Sambasivam, Susmitha Uppugalla, D Tejeswararao. "Nanohybrid material of Co–TiO2 and optical performance on methylene blue dye under visible light illumination", Hybrid Advances (Elsevier)., 2022, 1, 1-8.
8. P. Seetharam, Sathish Mohan Botsa. Physical, thermal, chemical and biological approaches for plastics degradation–A review, Cleaner Chemical Engineering (Elsevier)., 2025, 11, 100612.
9. Ezhilarasi, A., Vijaya, J.J., Kennedy, L.J., & Kaviyarasu, K. (2016). Green synthesis of NiO nanoparticles using Solanum trilobatum leaf extract for photocatalytic and antibacterial activity. Materials Science in Semiconductor Processing, 56, 98–104.
10. P. Vijaya Kumar, A. Jafar Ahamed, M. Karthikeyan, Synthesis and characterization of NiO nanoparticles by chemical as well as green routes and their comparisons with respect to cytotoxic effect and toxicity studies in microbial and MCF-7 cancer cell models, SN, Appl. Sci. 1 (2019)
11. M. Alagiri, S. Ponnusamy, C. Muthamizhchelvan, Synthesis and characterization of NiO nanoparticles by sol-gel method, J. Mater. Sci. Mater. Electron. 23 (3) (2012) 728–732.
12. Moradnia, F., Fardood, S. T., Zarei, A., Heidarzadeh, S., Ramazani, A., & Sillanpää, M. (2024). Green synthesis of nickel oxide nanoparticles using plant extracts: An overview of their antibacterial, catalytic, and photocatalytic efficiency in the degradation of organic pollutants. Iranian Journal of Catalysis, 14(1), 142401(1–24).
13. Prabhu, S., Thangadurai, T.D., Bharathy, P.V., &Kalugasalam, P. (2022). Synthesis and characterization of nickel oxide nanoparticles using Clitoria ternatea flower extract: Photocatalytic dye degradation under sunlight and antibacterial activity applications. Results in Chemistry, 4, 100285
14. Al-Zaqri, N., Umamakeshvari, K., Mohana, V., Muthuvel, A., &Boshaala, A. (2022). Green synthesis of nickel oxide nanoparticles and its photocatalytic degradation and antibacterial activity. Journal of Materials Science: Materials in Electronics, 33, 11864–11880. https://doi.org/10.1007/s10854-022-08149-1.
15. Saeed Kotb S, Ayoub IM, El-Moghazy SA, Singab ANB. Phytochemical analysis of Pithecellobium dulce (Roxb) Benth Bark via UPLC-ESI-MS/MS and evaluation of its biological activity. Nat Prod Res. 2024 Apr;38(8):1424-1429.
16. Preethi, S., & Mary Saral, A. (2014). GC–MS analysis of microwave-assisted ethanolic extract of Pithecellobium dulce. Malaya Journal of Biosciences, 1(4), 242–247.

17. Lakshmi, Y. S., Mala, D., Gopalakrishnan, S., Banu, F., Brindha, V., & Gajendran, N. (2014). Green synthesis and characterisation of silver nanoparticles from the medicinal plant Pithecellobium dulce. Indian Journal of Nano Science, 2(8),4-9.
18. Vincent, J., & Chandra Lekha, N. (2023). Green synthesis of gold nanoparticles using Pithecellobium dulce leaf extract and its biological activities. Chemical Engineering & Technology, 46(7), 1424–1431.
19. Kalaivani, P., & Mathubala, G. (2025). The Green Combustion Technique for Synthesizing CuO Nanoparticles with an Extract from Pithecellobium dulce Leaf: Potential Catalytic Activity. Asian Journal of Green Chemistry, 9(2), 151–166.
20. Raman, N., Sudharsan, S., Veerakumar, V., Pravin, N., & Vithiya, K. (2012). Pithecellobium dulce mediated extra-cellular green synthesis of larvicidal silver nanoparticles. Spectrochimica Acta Part A: Molecular and Biomolecular Spectroscopy, 96, 1031–1037.
21. N. Behera, M. Arakha, M. Priyadarshinee, B. S. Pattanayak, S. Soren, S. Jha and B. C. Mallick, Oxidative stress generated at nickel oxide nanoparticle interface results in bacterial, membrane damage leading to cell death, RSC Adv., 2019, 9, 24 888–24 894.
22. S. Srihasam, K. Thyagarajan, M. Korivi, V. R. Lebaka and S. P. R. Mallem, Phytogenic generation of NiO nanoparticles using Stevia leaf extract and evaluation of their in-vitro antioxidant and antimicrobial properties, Biomolecules, 2020, 10, 89–101.
23. M. I. Din and A. Rani, Recent advances in the synthesis and stabilisation of nickel and nickel oxide nanoparticles: A green adeptness, Int. J. Anal. Chem., 2016, 4, 1–14.
24. Firisa, S. G., Muleta, G. G., & Yimer, A. A. (2022). Synthesis of nickel oxide nanoparticles and copper-doped nickel oxide nanocomposites using *Phytolacca dodecandra*L'Herit leaf extract and evaluation of its antioxidant and photocatalytic activities. *ACS Omega, 7*(49), 44720–44732
25. Hosny, N. M. (2011). Synthesis, characterization and optical band gap of NiO nanoparticles derived from anthranilic acid precursors via a thermal decomposition route. *Polyhedron, 30*(3), 470–476.
26. Shukla RK, Yadav RK, Gole VL, et al. Band gap engineering of ADG/NiO nanocomposite and applications for photocatalytic reduction of nitrogen and photo-oxidation of dyes. *Main Group Chemistry*. 2024;23(3):329-345. doi:10.3233/MGC-240016
27. A.A. Ezhilarasi, J.J. Vijaya, K. Kaviyarasu, X. Zhang, L.J. Kennedy, Green synthesis of nickel oxide nanoparticles using Solanum trilobatum extract for cytotoxicity, antibacterial and photocatalytic studies, Surf. Interfaces 20 (Sep. 2020) 100553
28. N.A. Ludin, M.A.M. Al-Alwani, A.B. Mohamad, A.A.H. Kadhum, N.H. Hamid, M. A. Ibrahim, M.A.M. Teridi, T.M.A. Al-Hakeem, A. Mukhlus, K. Sopian, Utilization of natural dyes from Zingiber officinale leaves and Clitoria ternatea flowers to prepare new photosensitisers for dye-sensitised solar cells, Int. J. Electrochem. Sci. 13 (2018) 7451–7465, https://doi.org/10.20964/2018.08.04.
29. Ezhilarasi, A. A., Vijaya, J. J., Kaviyarasu, K., Maaza, M., Ayeshamariam, A., & Kennedy, L. J. (2016). *Green synthesis of NiO nanoparticles using Moringa oleifera extract and their biomedical applications: Cytotoxicity effect of nanoparticles against HT-29 cancer cells.Journal of Photochemistry and Photobiology B: Biology, 164,* 352–360.
30. E.R. Beach, K. Shqau, S.E. Brown, S.J. Rozeveld and P.A. Morris. Solvothermal synthesis of crystalline nickel oxide nanoparticles. Mater. Chem. Phys., 115, 371–377 (2009).
31. Venkata Nagendra Kishore, T., Jaya Prasanthi, K., Dendukuri, B. N. S. V., Seetharam, P., & Komara, J. (2025). *Dual functionality of cobalt doped nickel oxide nanoparticles in treatment of wastewater free from p-nitrophenol and microbes.International Journal of Environmental Sciences, 11*(6). ISSN: 2229-7359.
32. Singh, Y., Sodhi, R. S., Singh, P. P., & Kaushal, S. (2022). *Biosynthesis of NiO nanoparticles using* Spirogyra *sp. cell-free extract and their potential biological applications.Materials Advances, 3*(4991), 4991–5002.
33. R.K. Sharma, R. Ghose, Synthesis of porous nanocrystalline NiO with hexagonal sheet-like morphology by homogeneous precipitation method. Superlattices Microstruct. 80, 169–180 (2015)
34. A.-A. Salarian, Z. Hami, N. Mirzaei, S. M. Mohseni, A. Asadi, H. Bahrami, M. Vosoughi, A. Alinejad, M.-R. Zare, *J. Mol. Liq.*, **2016**, 220, 183–191.
35. Ahmad, B., Khan, M. I., Naeem, M. A., Alhodaib, A., Fatima, M., Amami, M., Al-Abbad, E. A., Kausar, A., Alwadai, N., Nazir, A., & Iqbal, M. (2022). Green synthesis of NiO nanoparticles using Aloe vera gel extract and evaluation of antimicrobial activity. Materials Chemistry and Physics, 288, 126363.
36. Sathishkumar, M., Sneha, K., Won, S. W., Cho, C. W., Kim, S., & Yun, Y. S. (2009). Cinnamon zeylanicum bark extract and powder mediated green synthesis of nano-crystalline silver particles and its bactericidal activity. Colloids and Surfaces B: Biointerfaces, 73(2), 332–338.